

*Journal of  
Mechanics of  
Materials and Structures*

**DYNAMICS OF A ROPE AS A RIGID MULTIBODY SYSTEM**

Paweł Fritzkowski and Henryk Kaminski

*Volume 3, N° 6*

*June 2008*

## DYNAMICS OF A ROPE AS A RIGID MULTIBODY SYSTEM

PAWEŁ FRITZKOWSKI AND HENRYK KAMINSKI

A preliminary discrete model of a rope is considered both as a scleronomic and a rheonomic system. Numerical experiments are performed and advantages of the applied algorithm are discussed on the basis of energy conservation. The problem of discretization of the rope is presented in terms of efficient computational simulations. A wave-like effect is discussed with regard to energy transfer and velocity of the model tip. The next directions of the model development are outlined.

### 1. Introduction

The dynamics of a rope may serve as an introduction to the problem of a cracking whip, which has been drawing the attention of scientists for over a hundred years. In the early twentieth century the hypothesis was advanced that the tip of the whip reaches supersonic speed at the crack time. Theoretical explanations of the phenomenon were supported later by numerous experiments, which in fact provided some surprising observations, for example the acceleration of the tip is up to 50000  $g$  and its velocity is about twice the speed of sound in the air [Pierański and Tomaszewski 2005].

Theoretical and experimental works focus not only on the motion of the whip. The dynamics of similar bodies, such as chains and ropes, is analyzed too. However, the results of the experiments cannot be confirmed by any accurate analytical calculations because of the complexity of the problem, which may be approximately described with the use of a complicated system of differential equations. Nevertheless, in such difficult cases computational methods may be very useful.

The papers by Pierański and Tomaszewski [2004; 2005] were the key papers for us on the initial stage of our work. The authors analyze the fall of a chain using a discrete model of the body. Goriely and McMillen [2002] consider the propagation and acceleration of waves in the motion of whips. Their paper is also a kind of introduction to the problem with its history outline.

We concentrate on a simple model, which actually is a rigid, chain-like model and more similar to the rope than the whip. Therefore, it plays a role of a preliminary model only, whose properties will be modified in the future. Applying the Lagrange formulation, we present the equations of motion for such a system both for the scleronomic and the rheonomic one. With the use of numerical methods we obtain an approximate solution to the problem. In several experiments we simulate the behaviour of the given body and analyze it mostly with respect to time dependencies of velocity and acceleration of the system's tip. Also some algorithmic matters of the simulations are considered.

### 2. Mechanical system and equations of motion

Below we define a discrete model of the rope, also used by Pierański and Tomaszewski [2005]. However, for us this model is introductory as mentioned before. The discussion is made more general by including the rheonomic case.

---

*Keywords:* multibody dynamics, discrete model, differential-algebraic equations, energy conservation.

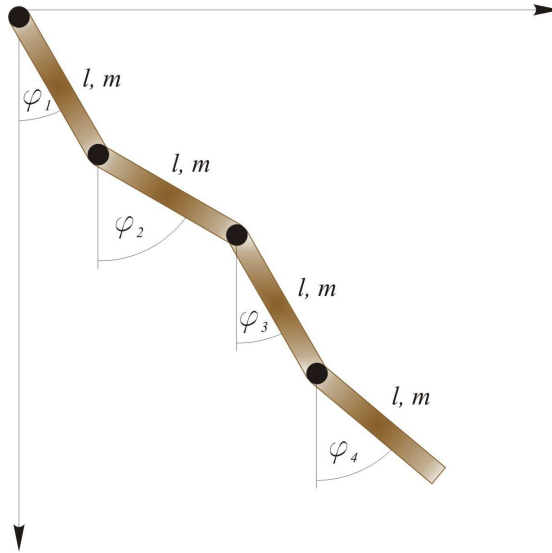


**Figure 1.** The simplest discrete model of the rope.

**2A. A system with scleronomic constraints.** Let us denote length of the rope by  $L$  and its mass by  $M$ . We divide the given body into  $n$  segments of length  $l$  and mass  $m$  each so that  $L = nl$  and  $M = nm$ . They are connected by ideal joints (without friction). Assuming that every element is a rigid cylindrical rod as well, we obtain the simplest discrete model of the rope which actually is a multiple physical pendulum (Figure 1).

We focus on a special case of a mechanical system moving in a gravitational field with no external forces acting on it. One end of the rope is attached to a stationary point whereas the other end moves freely. Furthermore, let us assume that the motion is restricted to take place in a vertical plane only.

To specify the state of the system we introduce angular generalized coordinates. The position of the  $i$ th element is described by a variable  $\varphi_i$  which defines the angle from the  $Y$  downward axis. The position of each segment (its mass centre) in the Cartesian coordinate system may be written as follows

$$x_i = \sum_{j=1}^{i-1} l \sin \varphi_j + \frac{1}{2}l \sin \varphi_i, \quad y_i = \sum_{j=1}^{i-1} l \cos \varphi_j + \frac{1}{2}l \cos \varphi_i, \quad (2-1)$$

and the velocities of the  $i$ th segment in the  $X$  and  $Y$  directions are expressed by the formulas

$$v_{xi} = \sum_{j=1}^{i-1} \dot{\varphi}_j l \cos \varphi_j + \frac{1}{2} \dot{\varphi}_i l \cos \varphi_i, \quad v_{yi} = - \sum_{j=1}^{i-1} \dot{\varphi}_j l \sin \varphi_j - \frac{1}{2} \dot{\varphi}_i l \sin \varphi_i.$$

Now we can write the kinetic energy of the whole mechanical system according to König's theorem

$$T = \frac{1}{2}m \sum_{i=1}^n v_i^2 + \frac{1}{2}I \sum_{i=1}^n \dot{\varphi}_i^2,$$

where  $I$  is the moment of inertia of each element ( $I = ml^2/12$ ). After some simplifications we obtain the kinetic energy in the following form

$$T = ml^2 \sum_{i=1}^n \frac{3(n-i)+1}{6} \dot{\varphi}_i^2 + ml^2 \sum_{i=1}^n \sum_{j=i+1}^n \frac{2(n-j)+1}{2} \dot{\varphi}_i \dot{\varphi}_j \cos(\varphi_i - \varphi_j).$$

The potential energy of the model is given by

$$V = -mg \sum_{i=1}^n y_i = -mgl \sum_{i=1}^n \frac{2(n-i)+1}{2} \cos \varphi_i.$$

Using the terms above for the Lagrangian  $L = T - V$  we can apply the Euler-Lagrange equations to describe behaviour of the system

$$\frac{d}{dt} \left( \frac{\partial L}{\partial \dot{\varphi}_i} \right) - \frac{\partial L}{\partial \varphi_i} = 0, \quad i = 1, 2, \dots, n. \quad (2-2)$$

After substitutions and simplifications we obtain the equations in the final form

$$\sum_{j=1}^n a_{ij} \ddot{\varphi}_j \cos(\varphi_i - \varphi_j) + \sum_{j=1}^n a_{ij} \dot{\varphi}_j^2 \sin(\varphi_i - \varphi_j) + \frac{g}{l} b_i \sin \varphi_i = 0, \quad i = 1, 2, \dots, n, \quad (2-3)$$

where

$$a_{ij} = \begin{cases} \frac{2(n-i)+1}{2}, & \text{for } j < i \\ \frac{3(n-i)+1}{3}, & \text{for } j = i \\ \frac{2(n-j)+1}{2}, & \text{for } j > i \end{cases} \quad \text{and} \quad b_i = \frac{2(n-i)+1}{2}. \quad (2-4)$$

To make it clearer, we present the equations of motion for  $n = 3$ :

$$\begin{aligned} a_{11} \ddot{\varphi}_1 \cos(\varphi_1 - \varphi_1) + a_{12} \ddot{\varphi}_2 \cos(\varphi_1 - \varphi_2) + a_{13} \ddot{\varphi}_3 \cos(\varphi_1 - \varphi_3) + a_{11} \dot{\varphi}_1^2 \sin(\varphi_1 - \varphi_1) \\ + a_{12} \dot{\varphi}_2^2 \sin(\varphi_1 - \varphi_2) + a_{13} \dot{\varphi}_3^2 \sin(\varphi_1 - \varphi_3) + (g/l) b_1 \sin \varphi_1 = 0, \\ a_{21} \ddot{\varphi}_1 \cos(\varphi_2 - \varphi_1) + a_{22} \ddot{\varphi}_2 \cos(\varphi_2 - \varphi_2) + a_{23} \ddot{\varphi}_3 \cos(\varphi_2 - \varphi_3) + a_{21} \dot{\varphi}_1^2 \sin(\varphi_2 - \varphi_1) \\ + a_{22} \dot{\varphi}_2^2 \sin(\varphi_2 - \varphi_2) + a_{23} \dot{\varphi}_3^2 \sin(\varphi_2 - \varphi_3) + (g/l) b_2 \sin \varphi_2 = 0, \\ a_{31} \ddot{\varphi}_1 \cos(\varphi_3 - \varphi_1) + a_{32} \ddot{\varphi}_2 \cos(\varphi_3 - \varphi_2) + a_{33} \ddot{\varphi}_3 \cos(\varphi_3 - \varphi_3) + a_{31} \dot{\varphi}_1^2 \sin(\varphi_3 - \varphi_1) \\ + a_{32} \dot{\varphi}_2^2 \sin(\varphi_3 - \varphi_2) + a_{33} \dot{\varphi}_3^2 \sin(\varphi_3 - \varphi_3) + (g/l) b_3 \sin \varphi_3 = 0. \end{aligned}$$

Having calculated all the coefficients according to (2-4) we obtain

$$\begin{aligned} \frac{7}{3} \ddot{\varphi}_1 + \frac{3}{2} \ddot{\varphi}_2 \cos(\varphi_1 - \varphi_2) + \frac{1}{2} \ddot{\varphi}_3 \cos(\varphi_1 - \varphi_3) + \frac{3}{2} \dot{\varphi}_2^2 \sin(\varphi_1 - \varphi_2) + \frac{1}{2} \dot{\varphi}_3^2 \sin(\varphi_1 - \varphi_3) + \frac{5}{2} (g/l) \sin \varphi_1 = 0, \\ \frac{3}{2} \ddot{\varphi}_1 \cos(\varphi_2 - \varphi_1) + \frac{4}{3} \ddot{\varphi}_2 + \frac{1}{2} \ddot{\varphi}_3 \cos(\varphi_2 - \varphi_3) + \frac{3}{2} \dot{\varphi}_1^2 \sin(\varphi_2 - \varphi_1) + \frac{1}{2} \dot{\varphi}_3^2 \sin(\varphi_2 - \varphi_3) + \frac{3}{2} (g/l) \sin \varphi_2 = 0, \\ \frac{1}{2} \ddot{\varphi}_1 \cos(\varphi_3 - \varphi_1) + \frac{1}{2} \ddot{\varphi}_2 \cos(\varphi_3 - \varphi_2) + \frac{1}{3} \ddot{\varphi}_3 + \frac{1}{2} \dot{\varphi}_1^2 \sin(\varphi_3 - \varphi_1) + \frac{1}{2} \dot{\varphi}_2^2 \sin(\varphi_3 - \varphi_2) + \frac{1}{2} (g/l) \sin \varphi_3 = 0. \end{aligned}$$

**2B. A system with rheonomic constraints.** Now let us assume that one end of the rope is attached to a moving support, whose position expressed in the Cartesian coordinates depends explicitly on time

$$x_0 = x_0(t) \quad \text{and} \quad y_0 = y_0(t).$$

The dependencies cause some modifications of the terms (2-1)

$$x_i = x_0 + \sum_{j=1}^{i-1} l \sin \varphi_j + \frac{1}{2}l \sin \varphi_i \quad \text{and} \quad y_i = y_0 + \sum_{j=1}^{i-1} l \cos \varphi_j + \frac{1}{2}l \cos \varphi_i. \quad (2-5)$$

Hence, the terms for the kinetic and the potential energy of the system have a more complex form:

$$\begin{aligned} T = ml^2 \sum_{i=1}^n \frac{3(n-i)+1}{6} \dot{\varphi}_i^2 + ml^2 \sum_{i=1}^n \sum_{j=i+1}^n \frac{2(n-j)+1}{2} \dot{\varphi}_i \dot{\varphi}_j \cos(\varphi_i - \varphi_j) \\ + \frac{1}{2}mn(\dot{x}_0 + \dot{y}_0)^2 + ml \sum_{i=1}^n \frac{2(n-i)+1}{2} \dot{\varphi}_i (\dot{x}_0 \cos \varphi_i - \dot{y}_0 \sin \varphi_i), \\ V = -mg \sum_{i=1}^n \left( \frac{2(n-i)+1}{2} l \cos \varphi_i + y_0 \right). \end{aligned}$$

Still using the general form of the dynamic equations (2-2), one may obtain their final form as follows:

$$\sum_{j=1}^n a_{ij} \ddot{\varphi}_j \cos(\varphi_i - \varphi_j) + \sum_{j=1}^n a_{ij} \dot{\varphi}_j^2 \sin(\varphi_i - \varphi_j) + b_i \frac{1}{l} (g \sin \varphi_i + \ddot{x}_0 \cos \varphi_i - \ddot{y}_0 \sin \varphi_i) = 0, \quad (2-6)$$

where  $i = 1, 2, \dots, n$  and the coefficients  $a$  and  $b$  are defined in (2-4).

It is important to remark that the described mechanical system is not a conservative one as its Lagrangian contains explicit time dependence because the transformation equations (2-5) involve the time explicitly.

### 3. Numerical experiments

The complexity of the presented dynamic equations and tending towards maximum possible number  $n$  of the model elements requires applying numerical methods to obtain an approximate solution to the problem.

In our analysis we have applied the MEBDFV code developed by Abdulla and Cash of Imperial College, London (Department of Mathematics). They implemented the modified extended backward differentiation formulas (MEBDF) of Cash. The algorithm is designed to solve stiff initial value problems for systems of linearly implicit differential algebraic equations (DAEs) of the form

$$\mathbf{M}(\mathbf{q})\dot{\mathbf{q}} = \mathbf{f}(t, \mathbf{q}), \quad (3-1)$$

where the matrix  $\mathbf{M}$  depends on  $\mathbf{q}$ , which is a vector of dependent variables, and  $t$  is the independent variable.

As is typical for computational methods, the system of dynamic equations should be reformulated as a system of first-order differential equations. Such a set of  $2n$  equations is presented below in matrix form with initial conditions

$$\begin{bmatrix} 1 & 0 & \dots & 0 & 0 & 0 & \dots & 0 \\ 0 & 1 & \dots & 0 & 0 & 0 & \dots & 0 \\ \vdots & \vdots & \ddots & \vdots & \vdots & \vdots & \ddots & \vdots \\ 0 & 0 & \dots & 1 & 0 & 0 & \dots & 0 \\ 0 & 0 & \dots & 0 & m_{11} & m_{12} & \dots & m_{1n} \\ 0 & 0 & \dots & 0 & m_{21} & m_{22} & \dots & m_{2n} \\ \vdots & \vdots & \ddots & \vdots & \vdots & \vdots & \ddots & 0 \\ 0 & 0 & 0 & 0 & m_{n1} & m_{n2} & \dots & m_{nn} \end{bmatrix} \begin{bmatrix} \dot{\varphi}_1 \\ \dot{\varphi}_2 \\ \vdots \\ \dot{\varphi}_n \\ \dot{\omega}_1 \\ \dot{\omega}_2 \\ \vdots \\ \dot{\omega}_n \end{bmatrix} = \begin{bmatrix} \omega_1 \\ \omega_2 \\ \vdots \\ \omega_n \\ f_1 \\ f_2 \\ \vdots \\ f_n \end{bmatrix}, \tag{3-2}$$

$$\varphi_i(t_0) = \varphi_{i0}, \quad \omega_i(t_0) = \omega_{i0}, \quad i = 1, 2, \dots, n.$$

The elements  $m_{ij}$  of the matrix  $\mathbf{M}$  depend on the generalized coordinates  $m_{ij} = a_{ij} \cos(\varphi_i - \varphi_j)$  with  $i, j = 1, 2, \dots, n$ , and the components  $f_i$  of the right-hand side vector are functions of the generalized coordinates as well as the generalized velocities

$$f_i = - \sum_{j=1}^n a_{ij} \omega_j^2 \sin(\varphi_i - \varphi_j) - b_i \frac{g}{l} \sin \varphi_i, \quad i = 1, 2, \dots, n.$$

For the rheonomic system, the terms for  $f_i$  contain the time as an explicit variable:

$$f_i = - \sum_{j=1}^n a_{ij} \omega_j^2 \sin(\varphi_i - \varphi_j) - b_i \frac{1}{l} (g \sin \varphi_i + \ddot{x}_0 \cos \varphi_i - \ddot{y}_0 \sin \varphi_i), \quad i = 1, 2, \dots, n.$$

In general, the applied solver carries out integration in three stages. Firstly, a solution at the current point is predicted and the Newton iterations are performed to improve the values. The next stage uses them to approximate a solution at the next point where the Newton scheme is applied again. The prediction process in the two phases involves the backward finite differences. The last stage plays a role of a corrector and is based on the Newton method again. The same Jacobian matrix is used in the iterations for all the three stages. Moreover, the code includes some strategy to reduce a number of the Jacobian evaluations. For more details on the usage of the modified backward differentiation formulas the reader is referred to [Cash and Considine \[1992\]](#).

First, we deal with the scleronomic system and discuss the simulations mostly from the algorithmic point of view. More physical aspects are taken into account when it comes to the rheonomic constraints. However, we focus only on the function  $x_0(t)$  referring to the horizontal direction. All the simulations are performed for the model of total length  $nl = 1$  m and total mass  $nm = 0.5$  kg. Additionally, zero generalized velocities are assumed at a start point  $\dot{\varphi}_i(0) = 0$  for  $i = 1, 2, \dots, n$ .

**Experiment 1.** We decided to confront results obtained in our numerical simulations with the results described in [Pierański and Tomaszewski \[2005\]](#) and based on the RADAU5 code developed by Hairer and Wanner. After performing the simulations for the scleronomic system with the same parameters ( $n, L, M$ ) and initial conditions, we analyzed configurations of the chain. As expected, there was no difference between the compared shapes of the multibody model in certain moments of time, and the time dependencies of the linear velocity of the tip were compatible too.

However, it was impossible to make a comparison between the results of motion in any longer time interval. Pierański and Tomaszewski focused on very short initial phases of the chain fall (from  $t = 0.0$  to  $t = 0.6$  s) which included the most interesting process namely the evolution of a sharp peak in the

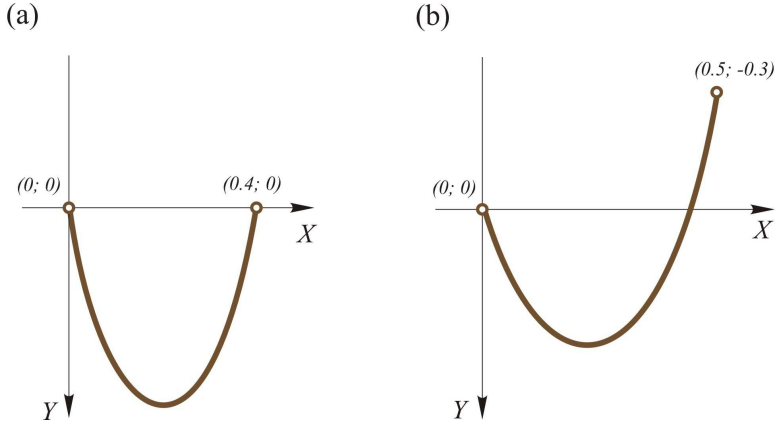


**Figure 2.** Initial configurations of the mechanical system. Left: Experiment 1; right: Experiment 2.

velocity time dependence of the tip. But even if they dealt with the farther stages, the agreement between the results could be not so good.

Actually, we applied the RADAU5 on the initial stage of our work. Aiming at simulations of the complex model motion in general (not only in a short time), we began to use the MEBDFV code. This was due to the character of the RADAU5, which is a solver for systems of DAEs with a constant matrix  $\mathbf{M}$ . A consequence of this is a problem with energy conservation of the model after a short period of good performance. Although one may update the matrix  $\mathbf{M}$  frequently, the results do not meet the energy conservation law. All in all, using the RADAU5 code without any significant modifications seems to be inefficient when researching long-lasting motion of such a complex mechanical system.

To show the difference, we performed a numerical experiment using both codes, with the same initial conditions for a catenary curve (Figure 2a) and the same parameters  $n = 20$ ,  $M = 0.5$  kg, and  $L = 1$  m.

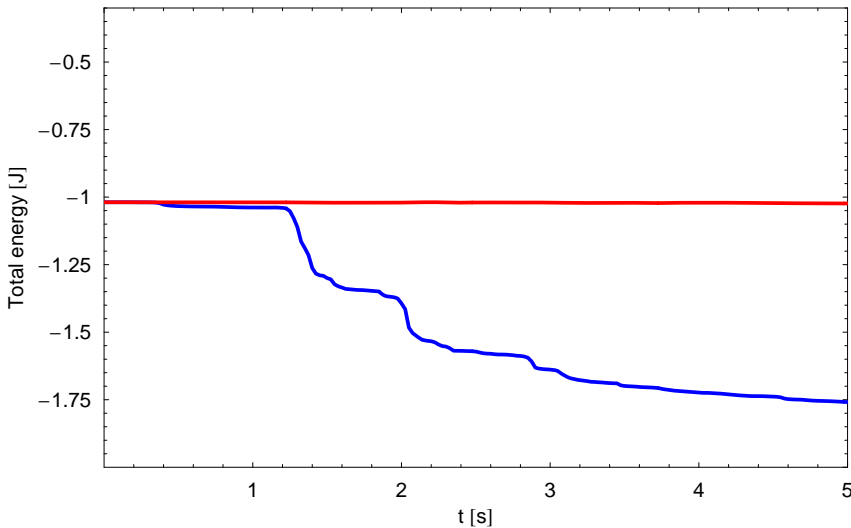


**Figure 3.** The total energy based on results from RADAU5 (blue) and MEBDFV (red).

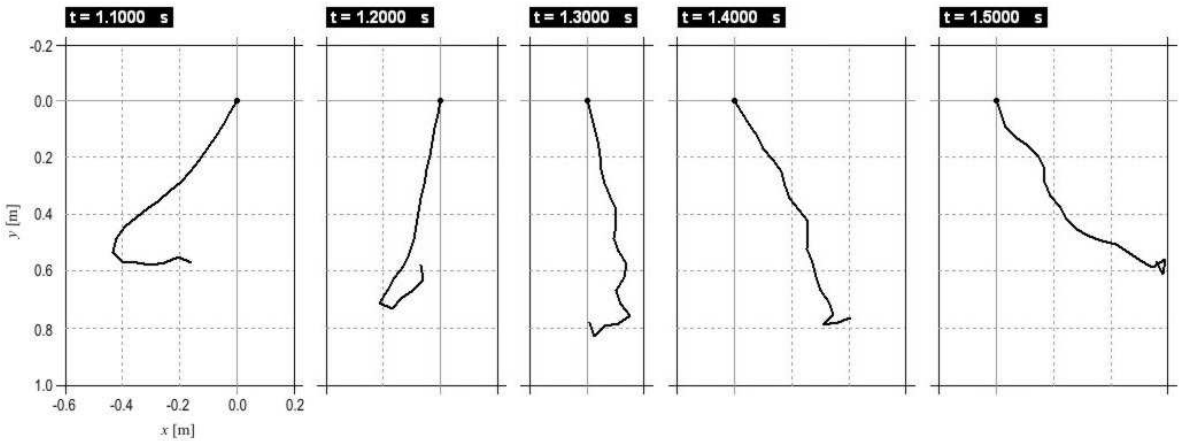


**Figure 4.** Configurations of the chain found in the numerical experiment with the use of the RADAU5.

Let us concentrate on the time dependence of the total energy of the model and its shape during the motion. According to Figure 3, the results obtained with the use of the RADAU5 show a rapid decrease in the energy around  $t = 1.3$  s. On the other hand, the red line illustrates the quantity given by the computation based on the other code—dependency with some small fluctuations (constant in the numerical sense). It may serve as the reference level for the former function. The difference between them increases with time and we can clearly see that the results provided by the solver RADAU5 do not meet the energy conservation law.

It is necessary to remark that no procedure designed for testing fulfillment of the conservation principle is embedded in the solvers. Both codes perform the integration process using some internal, numerical convergence tests, which do not refer to mechanics. The user supplies the physical meaning of the solution and involves it in the computation of such quantities as the total energy.

How do the energy losses affect the configurations of the chain? Are there any significant differences between the results again? To answer these questions we compare the configurations related to the RADAU5 code (Figure 4) and the MEBDFV code (Figure 5).

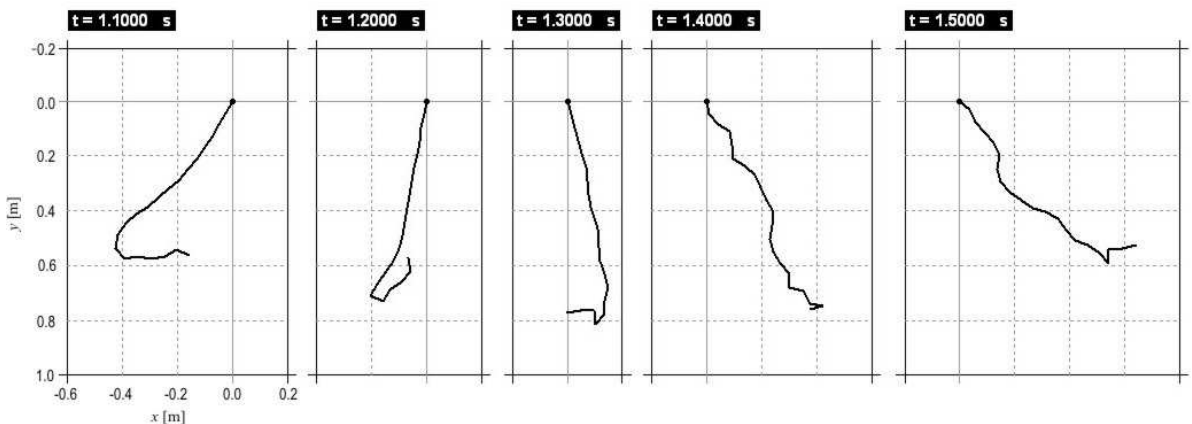


**Figure 5.** Configurations of the chain found in the numerical experiment with the use of the MEBDFV.

Although not all of the preceding configurations are presented, the shapes of the chain up to  $t = 1.2$  s are compatible. Some differences appear at point  $t = 1.3$  s and they intensify in time similarly to the ones between the energy dependencies. In general, the shapes of the first chain seems to be smoother, especially in the end phase of the experiment. In the second case, the constant total energy keeps the system going to a chaotic motion, which seems to be obvious when considering such a stiff multibody system. Therefore, the configurations of the latter chain become less and less ordered.

In the present work we do not deal with the theory of chaos and its application to dynamics of the chain, but we feel that this is an area which is worth further attention.

**Experiment 2.** Let us turn now to the problem of discretization of the rope. The question is how to match the number of the elements of the system to make our simulations efficient?

First, the model should reflect the real body with its physical features. Here we apply the discrete model (convenient in an algorithmic approach), which is to approximate the rope treated as continuum. Theoretically, reaching the idea of continuum is realized when  $n$  tends to infinity (and  $l$  tends to zero). In practice, it is possible and sufficient to choose some reasonably large number  $n$ .

However, it must be remembered that  $n$  defines a number of degrees of freedom, and thus the number of Lagrange-Euler equations of motion. In addition, from the numerical point of view the number is doubled when reformulating the system of equations as in (3-2). Thus, the number of the model elements affects the computation time considerably.

In the following experiment we do not specify any optimum. All we do is comparing configurations of the rope in simulations starting from the same initial conditions but from various  $n$ . Let us consider three cases:  $n = 30$ ,  $n = 45$ , and  $n = 70$ , with the same parameters  $M = 0.5$  kg,  $L = 1$  m, and the simulation time  $t = 2.5$  s. Initial configuration has the shape of a catenary curve (Figure 2b).

It is important to note that we omit the configuration of the rope at  $t = 0.5$  s, because the first phase of the motion for different number of segments  $n$  looks quite similar. We may say that the numerical integration of the dynamic equations related strictly to a fall of the chain proceeds without any serious problems. Some troubles appear in the next phase of motion, especially when the mechanical system tends to the chaotic-like behaviour. Usually the solver manages to go through the difficulties (it depends on the initial conditions) but it makes the computation time much longer.

First, we compare the shapes of the chain for  $n = 30$  and  $n = 45$  (Figure 6 and Figure 7). The two initial configurations seem roughly identical. However, there is a small difference. The free end of the model is located slightly lower in the second case (Figure 9). The reason of this is due to the

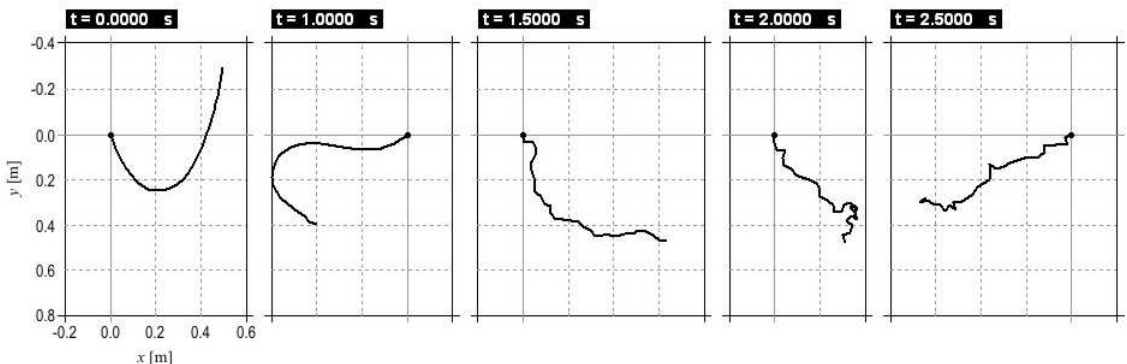


**Figure 6.** Configurations of the system consisting of  $n = 30$  segments.

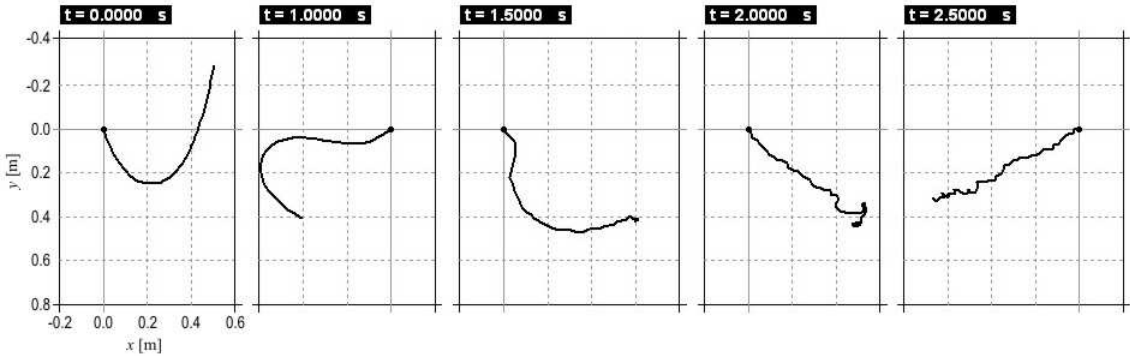


**Figure 7.** Configurations of the system consisting of  $n = 45$  segments.

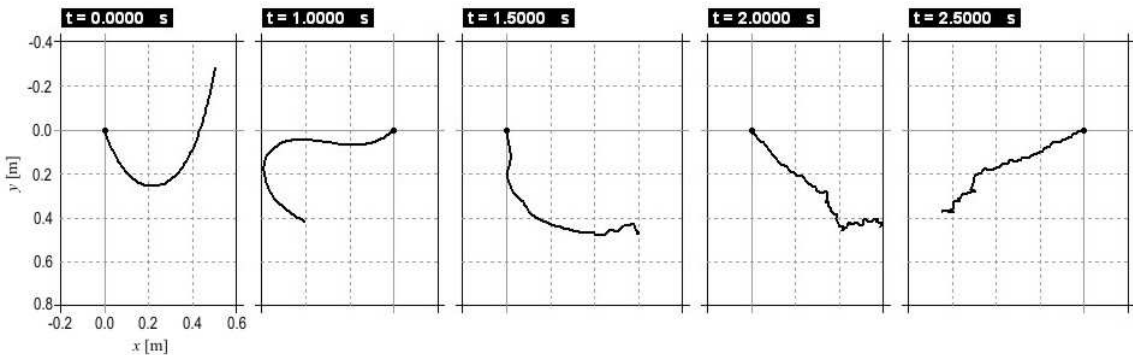


**Figure 8.** Configurations of the system consisting of  $n = 70$  segments.

discretization of the catenary which is hard to do without some small deviations. Nevertheless, it causes no noticeable differences at least for 1 s of the motion (the fall of the folded chain). We can see such differences from the third presented instant ( $t = 1.5$  s). As mentioned before, the end phase of the motion is chaotic-like. Therefore, the existing incompatibilities may be the effects of the discretization of the material continuum and/or slightly different initial conditions. The latter ones, in the chaotic dynamics, can produce even a completely new solution at later times.

Comparing the configurations for  $n = 45$  and  $n = 70$  (Figure 7 and Figure 8), we notice some differences at  $t = 1.5$  s again. However, they do not seem so evident. More significant ones are present in the next instant that is shown, and the last configurations differ from each other slightly.

To make our considerations more exact, we present the time dependence of the  $y$ -position of the models' tip (Figure 9). It should be emphasized that the dependence cannot be treated as a full measure of the quality of the solutions and their compatibility, since it refers just to one of the body's member (its free end). In addition, we have taken into account the  $Y$  direction only.

Obviously, the solutions to the problem for models with identical parameters but various numbers of segments  $n$  are more compatible for larger  $n$ . However, the number  $n$  does not have to tend to very large values. For example, if we presented results for  $n = 50$  and compared them with the ones for  $n = 70$ , no significant difference would be noticed. All in all, attempts to specify some reasonable limits of the discretization merit careful consideration.

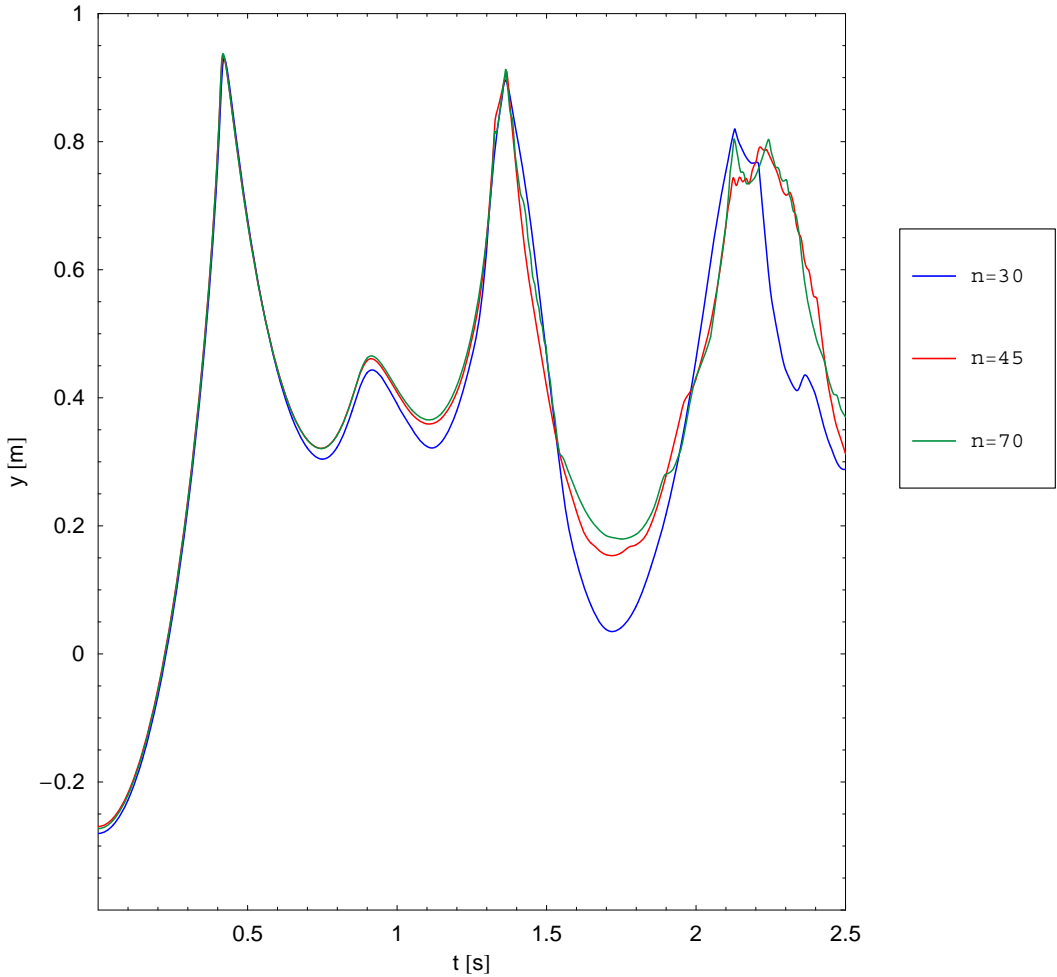


**Figure 9.** The  $y$ -positions of the chain tip for different number of segments.

**Experiment 3.** Now we turn to the rheonomic case and consider a free-hanging chain where the system resting at full extension so that  $\varphi_i(0) = 0$  for  $i = 1, 2, \dots, n$ . The body will be brought into motion with the use of the following constraint function

$$x_0(t) = A \sin^2(\pi B t), \quad (3-3)$$

where  $A$  and  $B$  are some constants. Here we take  $A = 0.1$  [m] and  $B = 5$  [1/s]. Actually, the attachment point is subjected to an oscillatory motion (Figure 10) with an amplitude  $A$ . We carry out simulations for two cases,  $n = 30$  and  $n = 50$ , which differ in the number of degrees of freedom.

Let us start the analysis with the time dependencies of the velocity and acceleration at the free end of the system consisting of  $n = 30$  segments. As presented in Figure 11, the significant amount of oscillations of the support produces numerous peaks in the tip velocity. However, the velocity increases slowly at the beginning and the first sharp peak occurs when the support velocity reaches its maximal value. The next peaks do not seem to be compatible with the  $v_{x_0}$  function, since the wave-like effects of the rheonomic constraints overlap in time and influence the tip motion with some delays.

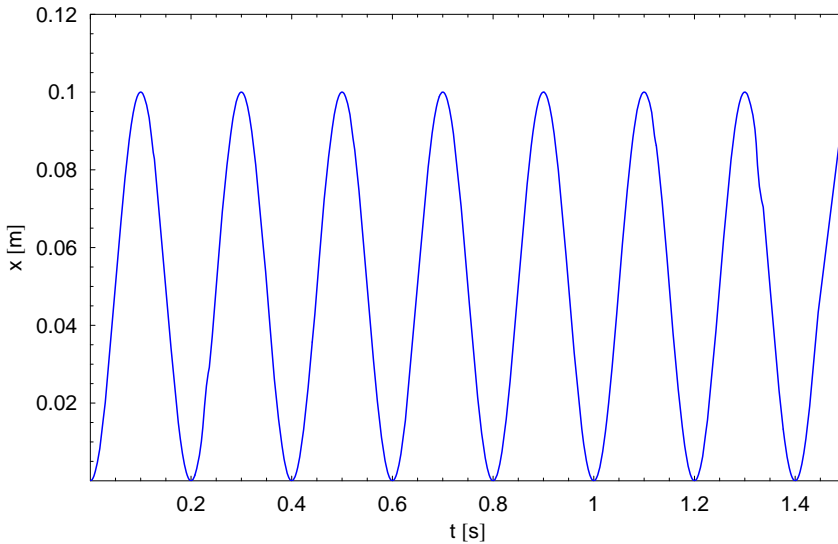


**Figure 10.** Constraint function  $x_0(t)$ .

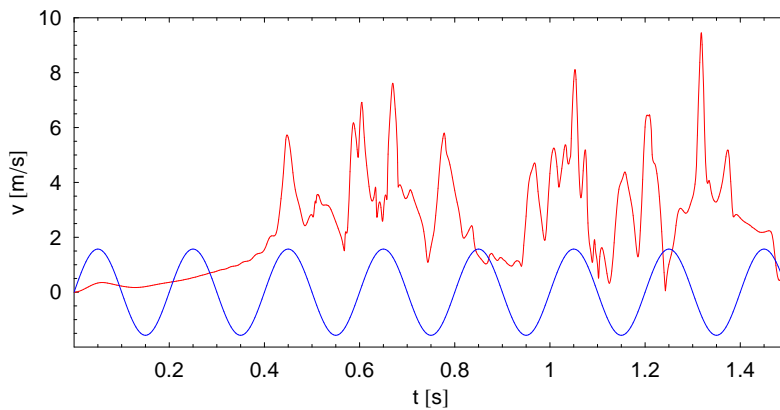


**Figure 11.** Velocity of the tip (red) and the function  $v_{x0}$  (blue) for  $n = 30$ .

Sharper peaks are visible in the acceleration dependency (Figure 12). They relate mostly to the maxima of velocity. An important conclusion arises from the graphs. Applying a very simple constraint function results in obtaining large values of the acceleration of the tip. For example, at time  $t = 0.68$  s the acceleration exceeds  $500 g$ .

To make the behaviour of the system more imaginable, we show particular phases of motion in Figure 13. It is easy to note that initially the free end of the chain moves upwards only. After four changes of direction of the support motion, in the time range  $t = 0.4$ – $0.5$  s the tip is pulled horizontally and its acceleration goes up suddenly. Obviously, there is a simultaneous increase in the velocity. The next phases are distinguished by growing disorder. In addition, just the tip seems to be a sort of origin of these effects. However, the details are considered later.

When it comes to the case with  $n = 50$  elements, the evolution of the rope motion looks quite similar. Nevertheless, the velocity and acceleration dependencies (Figure 14 and Figure 15) show more peaks

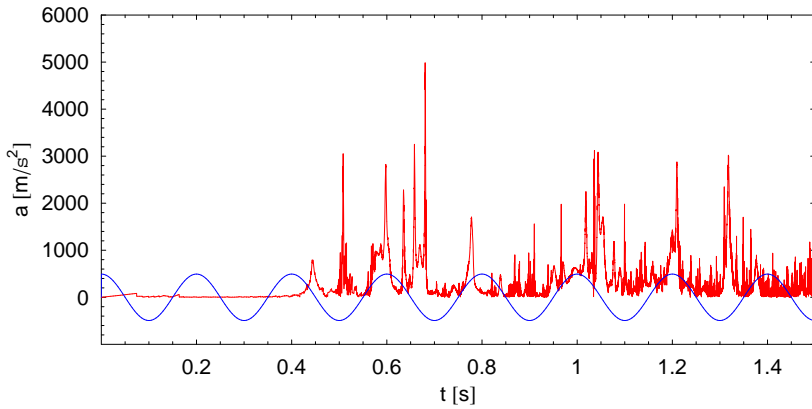


**Figure 12.** Acceleration of the tip (red) and the function  $a_{x0}$  times 10 (blue) for  $n = 30$ .

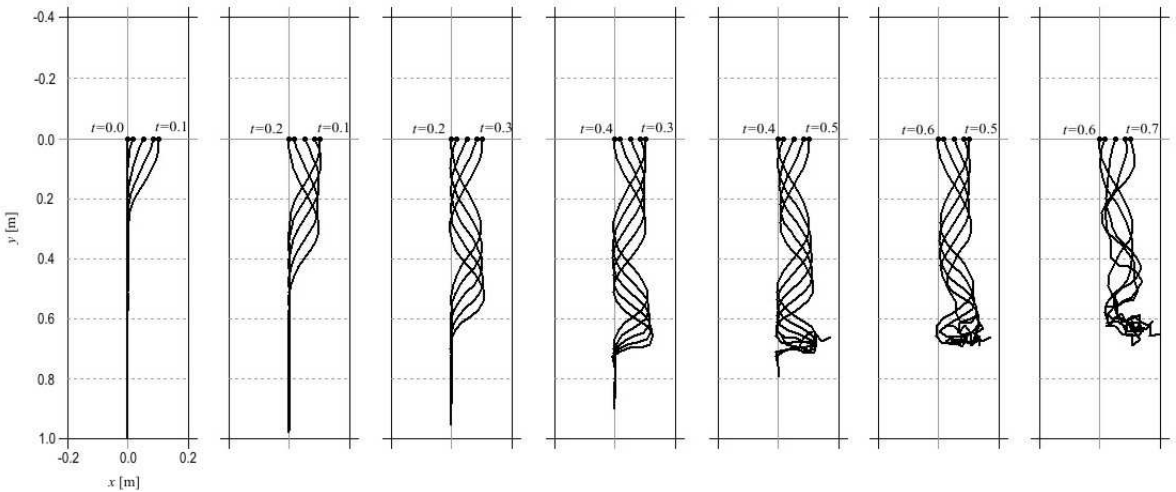


**Figure 13.** Configurations of the chain in consecutive phases of motion for  $n = 30$ . The time is given in seconds.

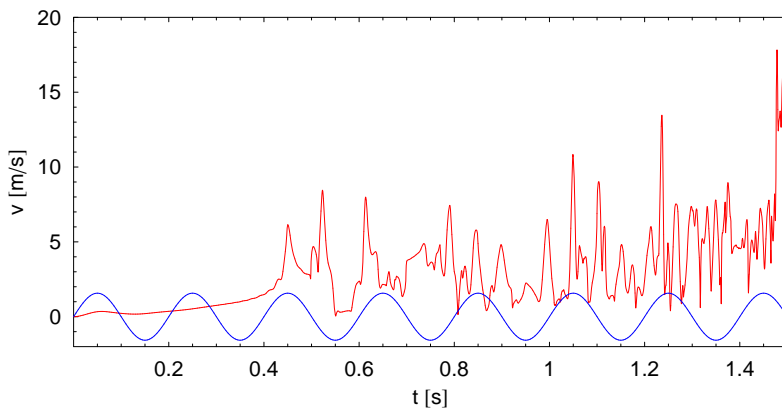


**Figure 14.** Velocity of the tip (red) and the function  $v_{x0}$  (blue) for  $n = 50$ .

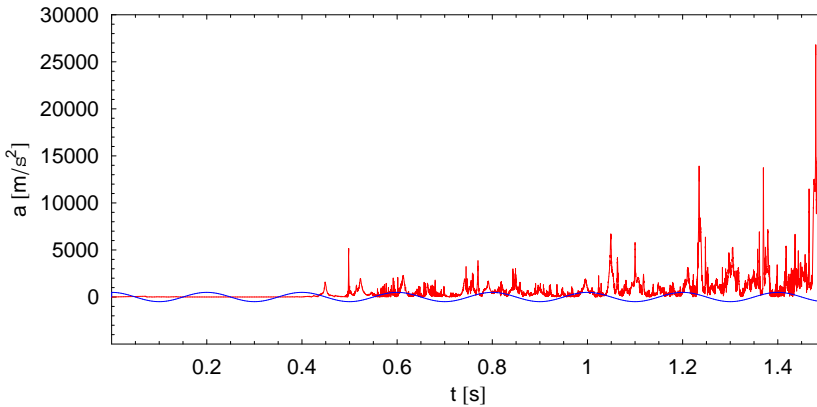


**Figure 15.** Acceleration of the tip (red) and the function  $a_{x0}$  multiplied by 10 (blue) for  $n = 50$ .

than before. The sharpest one occurs at the end of the simulation time in the chaotic-like phase. It should be remarked that the acceleration of the tip exceeds  $2500\text{ g}$  at this time.

Compared with the previous case, the configurations (Figure 16) are compatible during the ordered motion. Afterwards some differences appear (see  $t = 0.5\text{--}0.7\text{ s}$ ) and the degree of compatibility depends mainly on the difference between the number of segments in the two cases. This matter corresponds to the problem of discretization which we outlined in Experiment 2.

As mentioned, we expect the mechanical system to be nonconservative. Due to periodicity of the constraint function (3-3), energy is provided to the system all the time, except the moments when the support velocity  $v_{x0}$  equals zero. A graph of the total energy obtained from the approximate solution is presented in Figure 17. The irregular fluctuations on the advanced stage of motion have a numerical source, which may be also a result of the mechanical disorder.

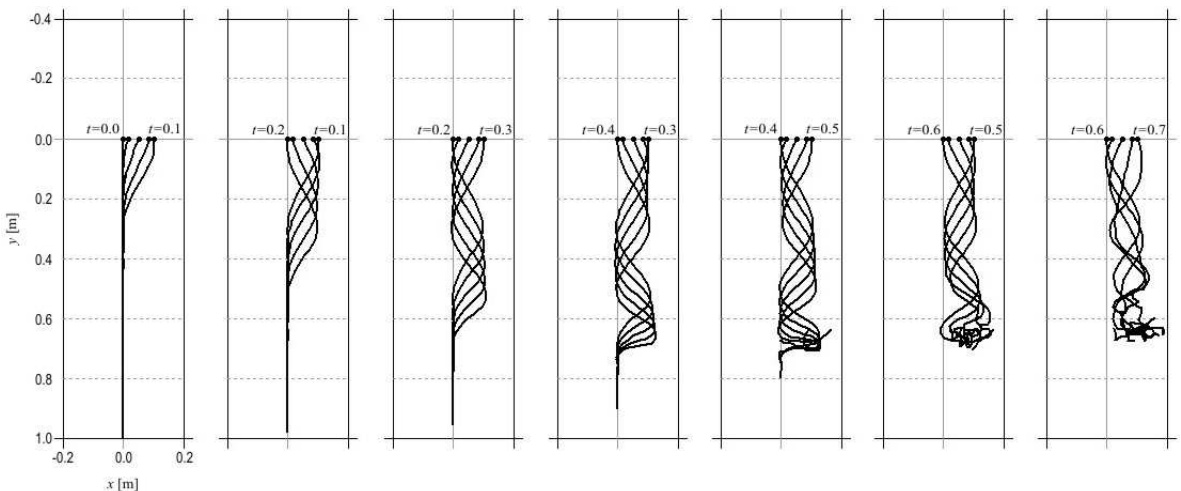


**Figure 16.** Configurations of the chain in consecutive phases of motion for  $n = 50$ . The time is given in seconds.

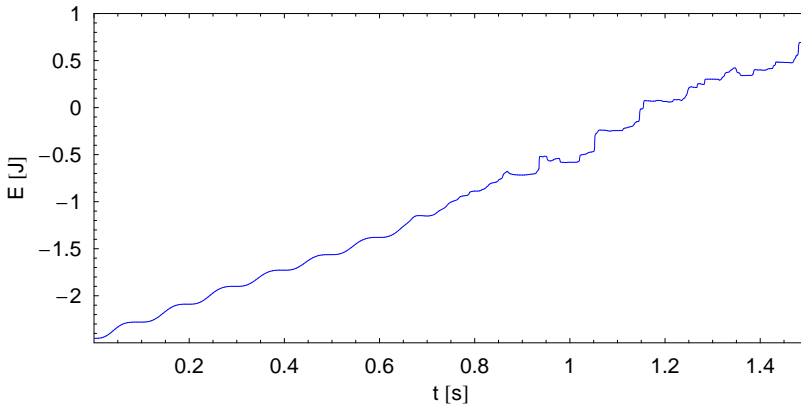


**Figure 17.** Total energy of the system with  $n = 50$  segments.

**Experiment 4.** This experiment is very similar to the previous one. However, here we wish to show some effects clearer. To do so, let us apply slightly different constraint function

$$x_0(t) = \begin{cases} A \sin^2(\pi B t) & \text{for } t \leq 1/B, \\ 0 & \text{for } t > 1/B, \end{cases}$$

where  $A$  and  $B$  remain the same, that is,  $A = 0.1$  [m] and  $B = 5$  [1/s]. In fact, there will be only one period in the support motion, after which its position will be stationary. The function is presented in [Figure 21](#). The initial configuration of the mechanical system is the same too  $\varphi_i(0) = 0$  for  $i = 1, 2, \dots, n$ . The number of degrees of freedom  $n$  is equal to 30.

In this case we begin our considerations with the chain's shape during the evolution. The two initial phases of motion ([Figure 18](#)) are identical with the ones from the Experiment 3. A considerable difference arises at the end of the support motion. A fold created from the upper part of the system is traveling along the rope and raising the tip gradually. After the downward propagation the last segments of the body rotate (the simple construction of the model allows them to do so) and a new fold is formed which

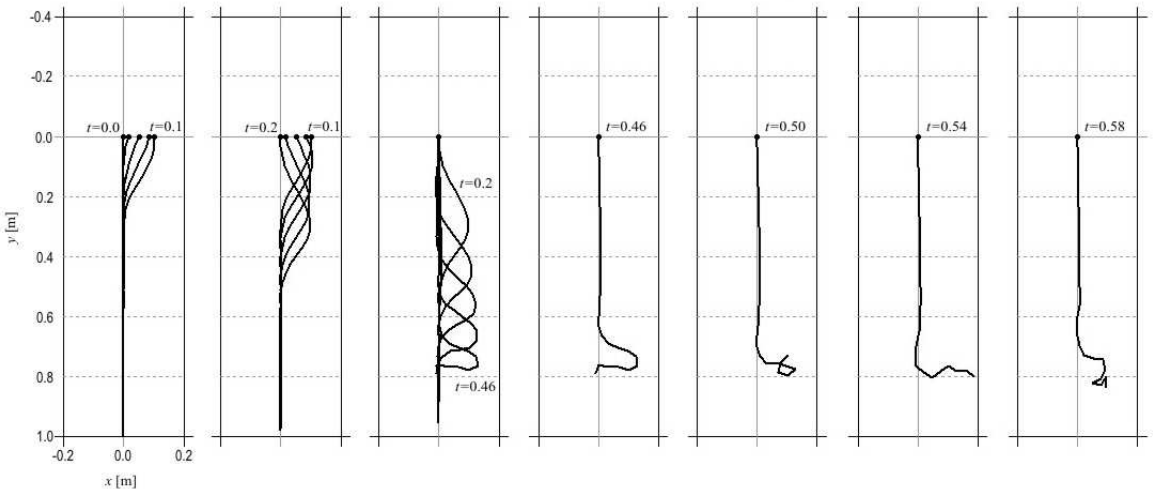


**Figure 18.** Downward travel of the fold (Experiment 4). Time given in seconds.

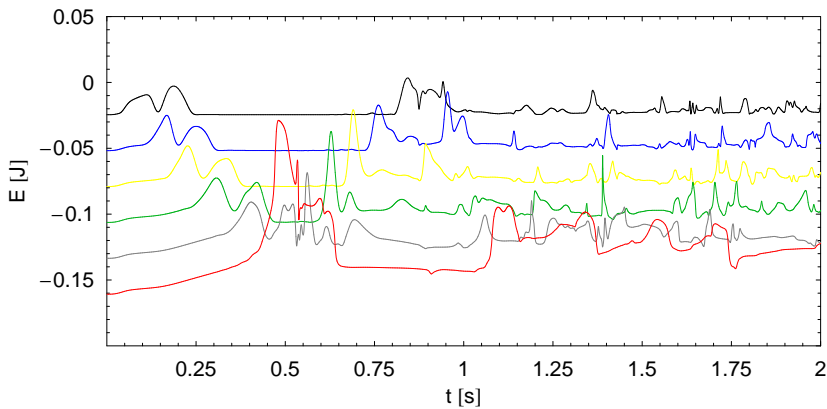


**Figure 19.** Total energy of the segments: 5 (black), 10 (blue), 15 (yellow), 20 (green), 25 (grey), 30 (red).

tends to go up ( $t = 0.6$  s). The upward travel is not so evident but the fold disappears completely just after the next direction change ( $t = 1.1$  s).

Actually, a similar situation was present in the previous simulations, but the periodic character of the  $x_0(t)$  function caused repetition and overlapping of such effects, which was confusing.

The fold travel seems to be a wave-like phenomenon. It should be remembered that in light of the existing explanations, a shock wave runs down the whip and carries energy which is cumulated on an increasingly smaller section of the whip. Finally, “as the length of this section decreases to zero, the end part of the tip moves with unbounded velocity and cracks as soon as it reaches the velocity of the sound in the air” [Goriely and McMillen 2002].

Although we do not expect such significant results, let us have a look at the energy dependencies. Figure 19 illustrates the flow of the energy along the rope. We choose only several segments but it is clear that as the wave goes down, it involves consecutive elements providing additional energy to them. The greatest increase of the total energy occurs at the last element. Moreover, the inversions of flow direction are visible too. After the second one the dependencies become less meaningful.

As it may be expected, there is a noticeable maximum in velocity of the tip which corresponds to the transfer of energy (Figure 20). The return of the traveling fold to the tip also results in a peak, however, it seems to start a specific series of similar peaks in the end phase of the simulation when the fold disappears.

Finally, we turn our attention to the total energy of the whole mechanical system (Figure 21). Initially, the magnitude increases in the manner presented in the previous experiment as long as the constraints depend on time. Afterwards the energy of the system remains constant at the level forced by the applied constraints. Thus, all the spectacular things connected to the wave-like effect happen in the state in which the total energy is conserved by the system.

#### 4. Conclusions

In the present work we have focused on the simple discrete model of the rope with two types of constraints, scleronomic and rheonomic. The multibody approach produces an expanded system of second order differential equations, which actually need to be solved numerically. Particularly in the case of the scleronomic constraints, the choice of the solver is justified by the energy principle. There is an

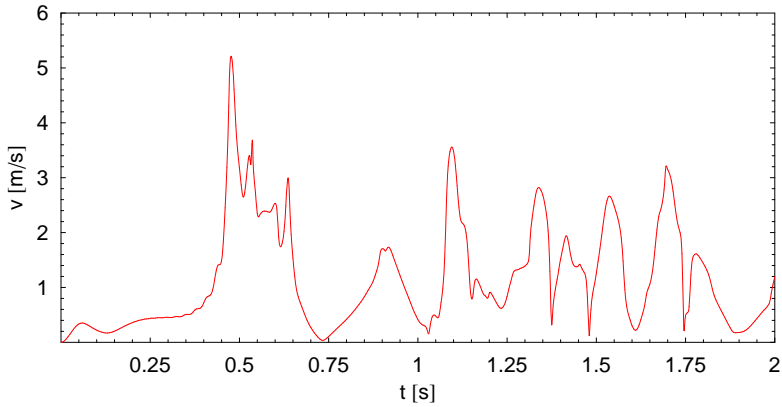


**Figure 20.** Velocity of the tip (Experiment 2).

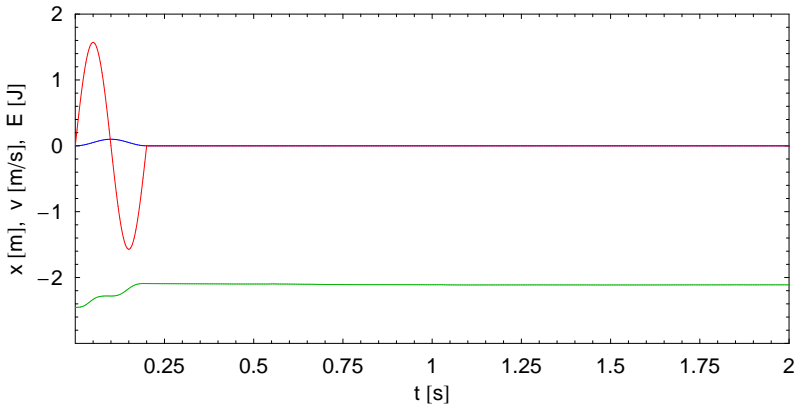


**Figure 21.** Total energy of the system (green) next to the constraint function  $x_0$  (blue) and its derivative  $v_{x_0}$  (red).

agreement between our results of computation and the results of the numerical and laboratory experiments presented in [Pierański and Tomaszewski \[2005\]](#). However, in order to perform computational simulations without significant energy losses (numerical dissipation) as well as rigorous restrictions related to time, we excluded the assumption that the left-hand side matrix in (3-1) is constant. Hence, the solutions to the problem obtained with the use of the MEBDFV code fulfill the energy conservation law in longer lasting motion.

We have also discussed the problem of discretization of the rope. The performed experiments point at possible improvements of the simulations' efficiency, in terms of shorter computation time and sufficient approximation of continuum by the model. Some reasonable limits of discretization, as an optimum of the number of elements, may not be very demanding when it comes to the computation capabilities.

As shown, the use of appropriate constraint functions results in emerging wave-like effects that are typical for the dynamics of the whip. The occurrence of sharp peaks in the time dependencies of velocity and acceleration of the tip turned out to be a result of the energy transfer between the consecutive elements of the discrete model.

In fact, the considered problem is a very good test for the applied solver. It seems that the code of Abdulla and Cash will succeed in solving dynamic equations for more complex mechanical systems including elasticity and damping. Also the function  $y_0(t)$  should be considered to perform various maneuvers moving the entire body and inverting its velocity. The air resistance and the chaotic dynamics are worth studying too.

All in all, the problem provides many possibilities of dynamics analysis, since the challenging multi-body approach in conjunction with computational methods give insight into numerous aspects of mechanics. Thus, we feel that the outlined directions of development are worth the efforts and will be realized successively.

### References

- [Cash and Considine 1992] J. R. Cash and S. Considine, “An MEBDF code for stiff initial value problems”, *ACM Transactions on Mathematical Software* **18**:2 (1992), 142–155.
- [Goriely and McMillen 2002] A. Goriely and T. McMillen, “Shape of a cracking whip”, *Phys. Rev. Let.* **88** (2002), #244301.
- [Pierański and Tomaszewski 2004] P. Pierański and W. Tomaszewski, “Fizyka strzelającego biczka”, *Foton* **85** (2004).
- [Pierański and Tomaszewski 2005] P. Pierański and W. Tomaszewski, “Dynamics of ropes and chains, I: The fall of the folded chain”, *New Journal of Physics* **7** (2005), #45.

Received 7 Feb 2008. Revised 26 Apr 2008. Accepted 26 Apr 2008.

PAWEŁ FRITZKOWSKI: [pawel.fritzkowski@gmail.com](mailto:pawel.fritzkowski@gmail.com)

*Computational Mechanics of Structures, Poznan University of Technology, Piotrowo 3, 60-965 Poznan, Poland*  
<http://www.fritzkowski.pl>

HENRYK KAMINSKI: [henryk.kaminski@put.poznan.pl](mailto:henryk.kaminski@put.poznan.pl)

*Institute of Applied Mechanics, Poznan University of Technology, Piotrowo 3, 60-965 Poznan, Poland*